A SEARCH FOR THE DETECTION OF HIGH ENERGY SOLAR NEUTRINOS IN THE ICECUBE DETECTOR

Thesis

Submitted to

The College of Sciences of

Southern University and A&M College

In Partial Fulfillment of the Requirements for

The Degree of

Master of Science in Physics

by

Cheng Guo

SOUTHERN UNIVERSITY AND A&M COLLEGE

Baton Rouge, Louisiana

December, 2012

This research was supported by a MRE grant from the National Science Foundation through a subcontract from the University of Wisconsin Board of Regents under the contract No. G067933. The author is also supported in part by the Air Force Office of Science Research under the contracts No. FA9550-09-1-0367 and FA9550-11-1-0330, and National Science Foundation under the contract No. CBET-0754821

A SEARCH FOR THE DETECTION OF HIGH ENERGY SOLAR NEUTRINOS IN THE ICECUBE DETECTOR

Name: Guo, Cheng

APPROVED BY:
(Chair of Department)

Ali R. Fazely, Ph.D
Chair of Committee

Diola Bagayoko, Ph.D
Committee member

Guang-Lin Zhao, Ph.D
Committee member

J. Gregory Stacy, Ph.D
Committee member

Dong-Sheng Guo, Ph.D
Committee member

Robert Miller, Ph.D
Dean of College of Sciences

Doze Y. Butler, Ph.D
Graduate School
Dean of Graduate School, Southern University

A SEARCH FOR THE DETECTION OF HIGH ENERGY SOLAR NEUTRINOS IN THE ICECUBE DETECTOR

Name: Guo, Cheng
Southern University and A&M College

Advisor: Dr. Ali R. Fazely

The IceCube Neutrino Telescope at the South Pole, completed in December of 2010, consists of 5160 Digital Optical Modules (DOMs) mounted on 80 vertical 1-km long strings arranged in a hexagonal pattern. Each string contains 60 DOMs located at a depth of 1450-2450 meters under the ice. The closely spaced inner arrays in the deepest ice, called DeepCore, enables the IceCube Neutrino Observatory to detect neutrinos at energies as low as 10 GeV. A special SN trigger based on a $\geq 6\sigma$ excess on top of the dark count-rate background in the DOMs is used to indicate a possible SN explosion. A close study of solar activities due to the onset of the solar cycle 24, revealed correlations between the IceCube Supernova trigger events and increased solar activities. In this thesis, we discuss these correlations and present the results and overall contribution of possible backgrounds due to the seasonal variation of the atmospheric muons. We conclude that these triggers are the results of high energy neutrino production in the sun. We expect the rate to increase with the maximum of the solar actvities in mid 2013 and subsequently drop afterwards.

ACKNOWLEDGEMENTS

The author would like to thank the Physics Department at Southern University for believing in him and giving him the opportunity to pursue his interest and goals in the areas of particle physics and astrophysics.

Special thanks are in order to Dr. Ali Fazely as advisor, for his considerable patience when explaining the theory and concepts, his insightful ideas and suggestions for the work contained herein, and for guiding, reviewing and correcting this thesis with expertise and patience, without which none of this work would be possible.

Thanks also to Dr. Samvel Ter-Antonyan for sharing the references concerning Solar and Neutrino astronomy, offering suggestion regarding this study and teaching programming skills.

He would like to thank Dr. Guang-Lin Zhao for offering him the opportunity to work on his project. The lab experience improved the author's experimental skills and consolidated data analysis.

Sincere thanks to all of the faculty: Dr. Pui-Man Lam, Dr. Dong-Sheng Guo, Dr. Laurence Henry for their guidance and assistance while a graduate student in the Physics Department.

TABLE OF CONTENTS

LIST OF TABLES

LIST OF FIGURES

CHAPTER I

INTRODUCTION

I.1 Statement of the Problem

The search for supernovae (SN) detection of neutrinos offers a unique tool to study various dynamical processes responsible for these cataclysmic events. SNs also provide a useful window to study the nature of neutrinos. The IceCube neutrino detector, although initially designed to detect high energy neutrinos, can also detect low energy neutrino bursts from the core collapse SNs. Low noise rate is attained with a huge amount of positrons originating from a large flux of $\bar{\nu}_e$ which induce a much higher count-rate over the background in all digital optical modules (DOMs). The detector's features and the methodology to search for SN burst trigger events will be discussed. The time interval for DOM rates is 2 ms. In order to re-bin and align the rates of individual modules, the IceCube collaboration has developed a histogramming program, enhanced by an analysis package that cleans, tests and records the data. Once the major construction was completed in December of 2010, IceCube became sensitive enough to cover 100% of supernovae in our galaxy. Being a member of the Supernova Early Warning System (SNEWS), the IceCube Detector makes a significant contribution to the observation of supernova neutrinos along with Super-K [2] and the Large Volume Detector (LVD) at Gran Sasso. [3]

The idea of the correlation between the increased rates in SN triggers and the increase in the sunspot activities was first noted and suggested in a Southern

University internal technical note [4] which was subsequently sent to the IceCube Supernova Working Group. The Southern Technote suggested that simultaneous solar activities, including sunspots, solar flux, x-ray and proton emissions are closely correlated with the increase in the sunspot activities based on a neutrino spectrum calculation proposed by Fargion Giacomo[5]. It can be concluded with high confidence that the SN triggers frequently observed in the IceCube data are in fact the result of high energy neutrinos ($> 100MeV$) interactions in the IceCube detector. These neutrinos are produced in the sun and are the result of an increase in the solar activities in the form of sunspots and x-ray/proton emissions due to the start of solar cycle 24.

The data analysis of the IceCube SN triggers in search of such events span from August of 2007 (solar minimum) through October 2012. The burn sample from the DeepCore was also studied which also confirmed the SN trigger increase.

I.2 Motivation for this Work

The SN trigger was designed to detect supernovae with the IceCube neutrino telescope. After a careful study of the increased rate in SN triggers, we proceeded to analyze the increase in the trigger rate with the increase of the sun activities due the onset of the Solar Cycle 24. The Monte Carlo (MC) analysis based of a high energy solar neutrino spectrum developed by Fargion and Giacomo[5] points to the fact that the SN trigger increase are because of high energy neutrinos captured by IceCube detector emanating from the Sun, and hence the high SN trigger rates are affected by solar activities correlated with the onset of the Solar Cycle 24. In this thesis we present evidence that a strong correaltion exists between the IceCube SN triggers and the increase in the sunspot activities. According to our data analysis, We believe the SN triggers will continue to increase when the solar cycle 24 reaches

its maximum in mid 2013.

I.3 Organization of Remainder of this Thesis

This thesis consists of five chapters which provide a comprehensive explanation for the detection of high energy solar neutrinos correlated with the increase in sunspot activities.

- **Chapter One** This chapter includes the introduction and statement of the problem, the motivation for the work, and a brief description of the contents of the thesis.
- **Chapter Two** This chapter gives a description of the Sun and the high energy solar neutrino production mechanism in detail.
- **Chapter Three** This chapter includes a discussion of the experimental setup and a description of the IceCube detector.
- **Chapter Four** This chapter contains the discussion of the observed neutrino trigger and its design and implementation. In-depth analysis of solar activities associated with sunspots and x-ray/proton emissions are also included.
- **Chapter Five** This chapter contains the conclusions and the summary of the results.

CHAPTER II

SUN AND SOLAR NEUTRINOS

II.1 Neutrino

A neutrino, denoted by the Greek letter ν, is an elementary particle that is electrically neutral, has a very small mass, and travels close to the speed of light. Neutrinos are the second most abundant particles in the universe, with photons being the most common. Neutrinos only carry weak interaction and gravity, consequently they have a very low reaction cross section which allows them to penetrate ordinary matter almost undisturbed. Most neutrinos passing through the Earth emanate from the Sun. The intensity of the solar neutrino flux on the Earth's surface is approximately 6.5×10^{10} neutrinos per $cm^2.s$. The IceCube detector is designed to probe the cosmos for very high energy neutrinos. It is also capable of seaching for MeV neutirnos from SN explosions

The neutrino was first postualted by Wolfgang Pauli in 1930. When observing the beta decay of an atomic nucleus into an electron and the recoil nucleus, physicists were puzzled by the fact that the electron, i.e. beta particle was not mono-energetic. Pauli proposed that there must be an undetected particle within the beta-decay scheme in accordance with the conservation of energy and momentum. [6] Enrico

$$N(n,p) \leftrightarrow N(n-1,p+1) + e^{-} + \bar{\nu}_e \tag{II.1}$$

Fermi developed the theory of beta decay in 1934, and named the yet to be detected particle proposed by Pauli, "neutrino" meaning "little neutral one" in Italian. The detection and confirmation came more than 20 years later, when Clyde Cowan and Frederick Reines published their discovery of neutrinos[7]. Fredrick Reines received the Nobel Physics prize in 1995 in both their names for their discovery of the neutrino.

Neutrinos are produced as a result of certain types of radioactive decay or nuclear reactions such as those which occur in the Sun, in nuclear reactors, particle accelerators or when cosmic rays collide with atomic nuclei. One well-known case is the emission of electron neutrino and/or its antiparticle, that is produced in nuclear beta decay when protons are changed into neutrons, or vice versa. There are three types or "flavors" of neutrinos: electron neutrino (ν_e), muon neutrino (ν_μ) and tau neutrino (ν_τ), named after corresponding leptons in the Standard Model; each type or flavor also has a corresponding antiparticle, called an antineutrino[8] (see table 1).

Table 1: Neutrinos and antineutrinos in the Standard Model of elementary particles

Fermion	Symbol	Mass
Generation 1		
Electron neutrino	ν_e	$< 2.0eV$
Electron antineutrino	$\bar{\nu}_e$	$< 2.0eV$
Generation 2		
Muon neutrino	ν_μ	$< 190keV$
Muon antineutrino	$\bar{\nu}_\mu$	$< 190keV$
Generation 3		
Tau neutrino	ν_τ	$< 18.2MeV$
Tau antineutrino	$\bar{\nu}_\tau$	$< 18.2MeV$

II.2 The Sun

Located at the center of the Solar System, the Sun is a near-perfect sphere and consists of hot plasma interwoven with magnetic fields. It has equatorial radius of about 6.955×10^8 m. The solar mass $M_\odot$ is 1.98892×10^{30} kg , and it accounts for about 99.86% of the total mass of the Solar System. [9] Based on spectral class, the Sun is classified as $G2V$. In the spectral class label, $G2$ indicates its surface temperature is approximately 5778 K and V indicates that the Sun, like most stars, is a main sequence star, and thus generates its energy by nuclear fusion of hydrogen nuclei into helium. The Sun travels through the Local Interstellar Cloud in the Local Bubble zone, within the inner rim of the Orion Arm of the Milky Way galaxy. The Sun orbits the center of the Milky Way at a distance of approximately 24k to 26k light years from the galactic center, completing one clockwise orbit in approximately 220,000,000 years. Since our galaxy is moving with respect to the cosmic microwave background radiation (CMB) in the direction of the constellation Hydra with a speed of 550 km/s, the sun's resultant velocity with respect to the CMB is about 370 km/s in the direction of the Crater or the Leo constellation. [10]

In the Standard Solar Model (SSM), the Sun is mathematically treated as a spherical volume of gas (in varying states of ionization, with the hydrogen in the deep interior being completely ionized plasma). This model is described by several differential equations derived from basic physical principles with boundary conditions, namely the luminosity, radius, age and composition of the Sun, which are well determined. The SSM is used to test the validity of stellar evolution theory, and it serves two purposes: to provide estimates for the helium abundance and mixing length parameter by forcing the stellar model to have the correct luminosity and radius at the Sun's age; and to provide a way to evaluate more complex models with additional physics, such as rotation, magnetic fields and diffusion or

improvements to the treatment of convection, such as modeling turbulence, and convective overshooting.[11] To make the SSM fit observations, one must determine the two free parameters of the stellar evolution model—the helium abundance and the mixing length parameter (used to model convection in the Sun). The SSM changes over time to be consistent with relevant new theoretical or experimental physics discoveries. In order to simulate the solar models, one utiliazes the input from various parameters randomly drawn for each model from separate probability distributions for each parameter [12].

The Sun is composed primarily of the chemical elements hydrogen and helium; they account for 74.9% and 23.8% of the mass of the Sun in the photosphere, respectively.[13] All heavier elements account for less than 2% of the mass. The most abundant heavy elements are oxygen (roughly 1% of the Solar mass), carbon (0.3%), neon (0.2%) and iron (0.2%).[14] The Sun inherited its chemical composition from the interstellar medium out of which it was formed. H and He in the Sun were produced by the Big Bang nucleosynthesis. The metals were produced by stellar nucleosynthesis in generations of stars which completed their stellar evolution and returned their materials to the interstellar medium before the formation of the Sun.[14] The chemical composition of the photosphere is normally considered representative of the composition of the primordial Solar System.[15] However, since the Sun formed, the helium and heavy elements have settled out of the photosphere. Therefore, the photosphere now contains slightly less helium and only 84% of the heavy elements than the protostellar Sun did; the protostellar Sun was 71.1% hydrogen, 27.4% helium, and 1.5% heavy elements. [13] In the inner portions of the Sun, nuclear fusion has modified the composition by converting hydrogen into helium, so the innermost portion of the Sun is now roughly 60% helium, with the heavy element abundance unchanged.

In the study of the structure of the Sun, solar physicists separate it into four

domains: the interior, the surface atmospheres, the inner corona, and the outer corona. The Sun's interior domain includes the core, the radiative layer, and the convective layer (Figure II.1).

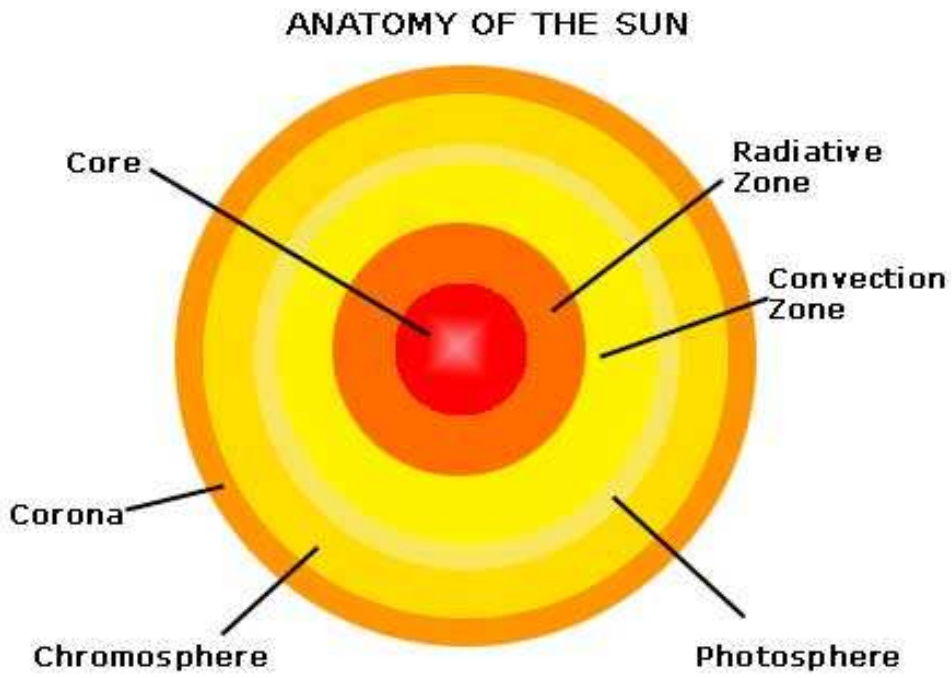

Figure II.1: The Structure of the Sun

The core is the source of the solar energy, the site of thermonuclear fusion. At a temperature of about 1.5×10^7 K, matter exists in the state of plasma where atomic nuclei (principally protons) and electrons are moving at very high speeds. Under these conditions nuclear fusion occurs, which results in the formation of heavier elements as well as the release of energy in the form of gamma ray photons as well as neutrinos. The next layer out from the core is the zone that emits huge amounts of radiation which diffuse outward. The temperature ranges from 15 million K to one million K. The gamma photons, produced by fusion in the core, are absorbed and re-emitted repeatedly by nuclei in the radiative layer, with the re-emitted

photons having successively lower energies and longer wavelengths. Above the radiative layer is the convective layer which has lower temperatures and less radiation. Energy is transported outward mostly by convection. Convective circulation of plasma (charged particles) generates large magnetic fields that play an important role in producing sunspots and flares. The solar surface atmospheres are composed of the photosphere and the chromosphere. The photosphere is the part of the Sun that produces most of the visible (white) light. Bubbles of hotter material well up from within the Sun, dividing the surface of the photosphere into bright granules that expand and fade in several minutes, only to be replaced by the next upwelling. The photosphere is one of the coolest layers of the Sun; its temperature is about $6000K$. Sometimes huge magnetic-field bundles break through the photosphere, disturbing this boiling layer with a set of conditions known collectively as solar activity. The magnetic fields create cooler, darker regions, known as sunspots. The chromosphere lies just above the photosphere, and is slightly cooler at its base. But when viewed only in the red light produced by hydrogen (called Hα), the chromosphere is seen to be alive with many distinctive features, including long dark filaments and bright areas known as pelage that surround sunspot regions. The Corona is the outer layer of the Sun's atmosphere, and it extends for millions of kilometers and the temperatures are tremendous, reaching one million K. Holes in the corona occur where the Solar magnetic field loops out into space. These coronal holes may be the source of the solar wind, a stream of energetic particles that permeate the Solar System.

II.3 Solar Cycle

The amount of magnetic flux that rises up to the Sun's surface varies with time in a cycle called the solar magnetic activity cycle, or solar cycle for short. This cycle

lasts 11 years on average. The cycle is sometimes referred to as the sunspot cycle. Near the minimum of the solar cycle, it is rare to see sunspots, and the spots that do appear are very small and short-lived. However, during the "solar maximum", there are sunspots visible almost all the time (often there are over 100 spots visible at a time), and some of those spots will be very large (up to 50,000 km in diameter) and last several weeks. There was a sunspot maximum in 2000-2001 and we expect another in mid 2013.

II.4 Solar Fusion and Neutrinos

There are two sets of nuclear fusion in the Sun, one is the CNO cycle (for carbon-nitrogen-oxygen), also known as Bethe-Weizsacker-cycle, which makes stars convert hydrogen to helium, the other being the p-p chain (proton-proton chain). Unlike the p-p chain reaction, the CNO cycle is a catalytic cycle as shown in Figure II.2

Theoretical models show that the CNO cycle is the dominant source of energy in stars more massive than about 1.3 times the mass of the Sun. For stars the mass of the Sun or less, the p-p chain is more important. The net p-p reaction is

$$4p + 2e \rightarrow He + 2\nu_e \tag{II.2}$$

And the complete p-p chain is shown in figure II.3

As a consequence of the p-p chain reaction, most solar neutrinos are produced as a product of nuclear fusion, and have a low energy, up to 400 keV. There are also several other significant production mechanisms, with energies up to 18 MeV as shown in figure II.4.

Solar neutrino flux detection is very important not only for the understanding of the stellar evolution but also for the study of the origin of the solar activity cycle.

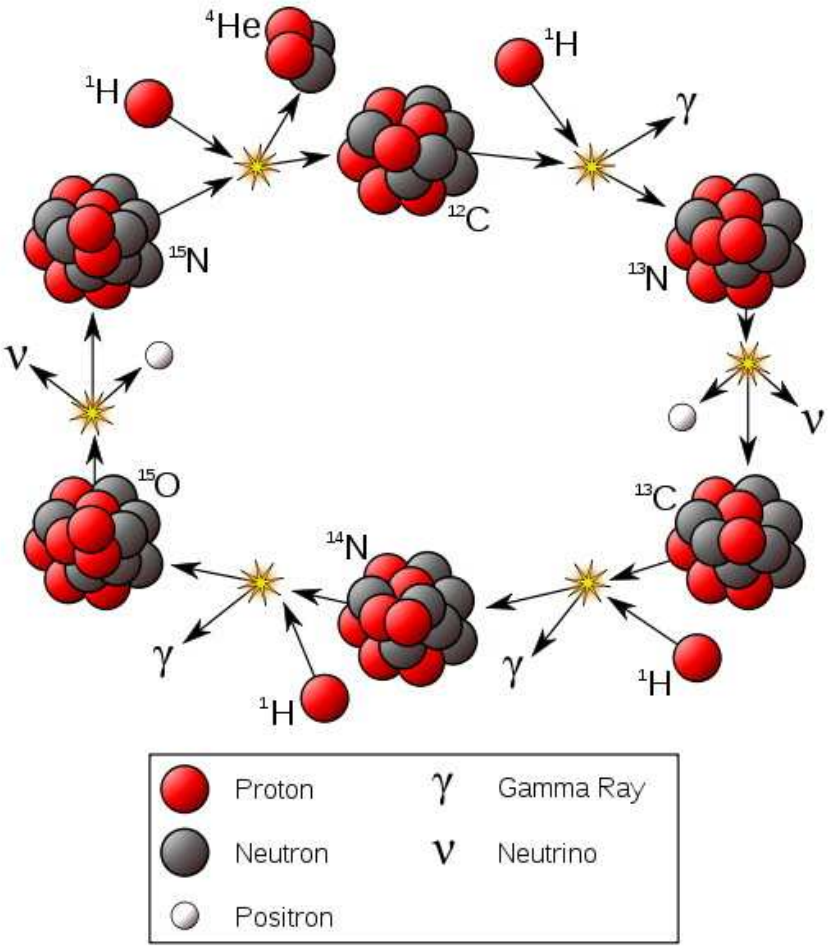

Figure II.2: Overview of the CNO-I Cycle

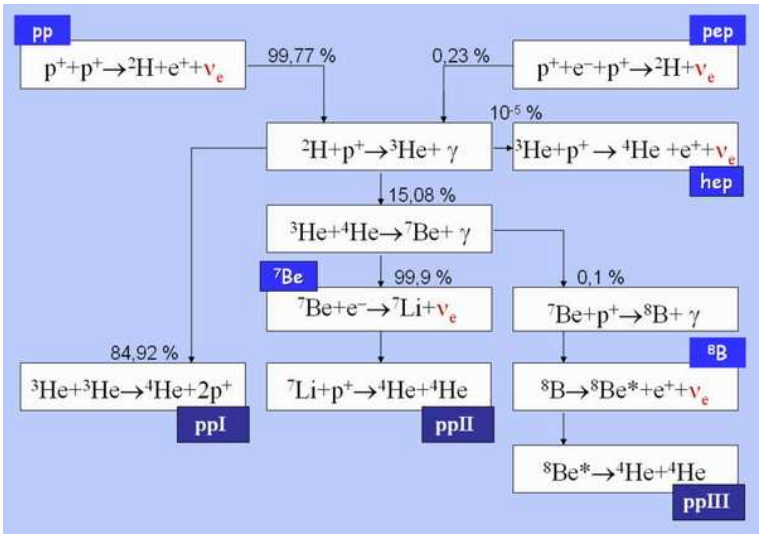

Figure II.3: Solar neutrinos (proton-proton chain) in the Standard Solar Model

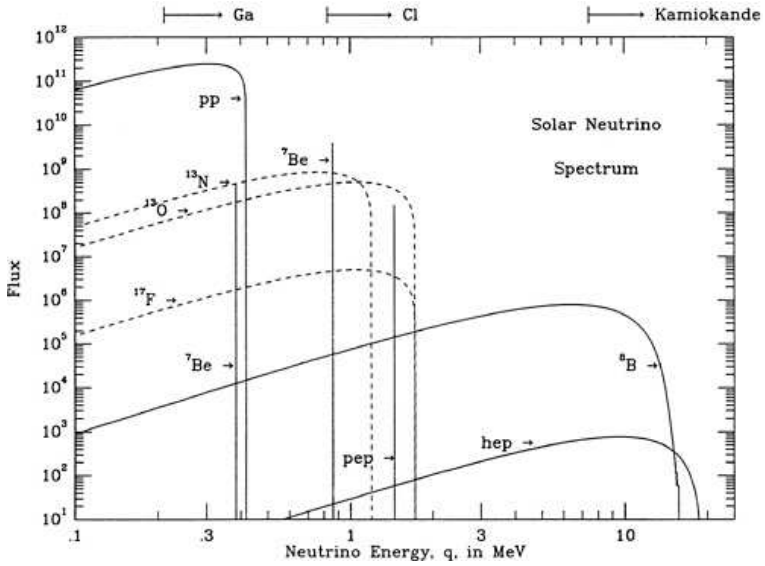

Figure II.4: The solar neutrino spectra predicted by the Standard Solar Model

The number of neutrinos predicted by the SSM are much higher than the actual detected number of the solar neutrinos. Various experiments [1] have shown that the number of detected neutrinos are between 1/3 and 1/2 of that of the predicted flux. This was known as the solar neutrino problem. The Super-Kamiokande

Collaboration announced the first evidence of neutrino oscillation in 1998.[2] It produced observations consistent with muon-neutrinos (produced in the upper atmosphere by cosmic rays) changing into tau-neutrinos. A more significant discovery was made in 2001 from the Sudbury Neutrino Observatory (SNO) in Canada[17], producing the direct evidence of neutrino oscillation. According to extensive analysis, 35% are electron-neutrinos, and the rest are muon- and/or tau-neutrinos. This is consistent with the number of solar neutrinos predicted by the SSM.

CHAPTER III

EXPERIMENTAL ARRANGEMENT

III.1 The IceCube Detector

The IceCube detector, located at the Geographic South Pole, detects high energy neutrinos that traverse the earth and interact deep in the ice below the south pole. Particles such as muons, electrons, and hadrons produced by charged-current(CC) or neutral-current (NC) neutrino interactions generate Cherenkov light that can be detected by an array of DOMs.

Deep water filled holes were created by melting the ice with a hot water drill and strings of DOMs were then lowered into the holes. IceCube instruments 1 km^3 of ice using DOMs deployed on 78 strings on a 125 m hexagonal grid. Each string contains 60 modules with a 17 m spacing at depths ranging from 1450 m to 2450 m. The first string was deployed in January 2005 and a total of 78 strings are presently deployed. Each DOM consists of a 13-inch diameter pressure vessel containing a Hamamatsu R7081-02, 10-inch diameter PMT, PMT base, high voltage supply and signal processing and calibration electronics. The main board includes trigger and front-end electronics, two analog-to-digital converter (ADC) systems, a precision clock and a large Field Programmable Gate Array (FPGA) for control and communications. All communications with the surface are through a simple twisted-pair cable shared by two DOMs. This simple pair carries power, bi-directional data and timing calibration signals. The PMT signal is AC coupled

with a transformer on the base and then sent to a discriminator and two separate digitizer circuits. The firing of the discriminator, typically set for 1/3 of a photoelectron pulse, initiates a digitization cycle. The first digitization, based on a custom switched-capacitor-array chip, provides 14 bits of resolution. The other digitizer system detects late arriving light which was scattered in the ice. A second board holds 12 Light Emitting Diodes (LED) that are used for calibration. Half of the LEDs point horizontally outward while the other half point upwards at 45 degrees. A surface air-shower array, called IceTop, has two detector tanks above each in-ice string. Each 2.7 m diameter ice-filled tank contains two DOMs. IceTop can be used to help calibrate IceCube and as a veto as well as serving as an air-shower detector.

Modeling of the performance of IceCube depends crucially on a detailed understanding of the optical properties of the ice. AMANDA mapped scattering and absorption of the glacial ice at the South Pole for wavelengths between 313 and 560 nm at depths between 1100 m and 2350 m. Significant variations with depth were observed, as much as a factor of seven for scattering in the depth range of the IceCube DOMs. The absorption length of the ice is very long, typically 100 m, while the effective scattering length is short, typically 20 m. This is in contrast to water detectors, such as ANTARES where scattering lengths are long (≈100m) and absorption lengths short (≈20m) [19].

Scattering of light in the ice is strongly forward peaked so that several collisions are needed to substantially change the photon direction. This suggests the usefulness of the effective scattering length, $Ł_{eff} = L_s/(1- < cos(\theta) >)$ where L_s is the mean distance between scatters and $< cos(\theta) >$ is the average cosine of the angle of scatter. Very qualitatively, $Ł_{eff}$ is the distance required to substantially change the direction of the photon. It can be shown that scattering is well described by the single parameter, $Ł_{eff}$, for distances large compared to $Ł_{eff}$. The distance

light needs to travel to reach a DOM in IceCube is typically larger than Ł$_{eff}$ and thus the directional information of much of the Cherenkov light is lost.

The direction of a high energy muon can still be determined with high accuracy since the muon track is long. Due to scattering, photons that reach a DOM typically do not take the shortest path to the DOM and thus arrive delayed by a time $t_{residual}$. The angular resolution of IceCube is approximately one degree at high energies. Electromagnetic and hadronic showers are short, typically 10 to 20 meters, and thus the direction can only be determined to about 30 degrees, but containment allows a better energy measurement than that of muons.

The energy threshold for IceCube is approximately 100 GeV. The trigger rate is approximately 80 Hz and all events with 23 optical modules firing with 2.5 μs are recorded. This yields approximately 10^9 events each year, primarily down-going muons arising from decay of pions and kaons produced by cosmic ray interactions in the atmosphere. Approximately 10^6 of these down-going muons are mis-reconstructed as upward-going muons. Mis-reconstructed down-going muons constitute the main background for this neutrino sample and fairly elaborate software cuts are required to reduce the muon background to an acceptable level. Most of the neutrinos detected are atmospheric neutrinos and these provide a very useful calibration sample for IceCube, but they also constitute a background when searching for extraterrestrial sources of neutrinos.

III.2 The DeepCore

IceCube, with its sparse distribution of DOMs over a large volume of ice is optimized for the detection of high energy neutrinos. There is, however, significant interest in the IceCube collaboration in having a region of the detector that is sensitive at low energies for WIMP searches, studies of neutrino oscillations and other phenomena. A

low energy extension of IceCube, called DeepCore (DC), has eight (8) strings located in the central region of IceCube. Each DC string has 60 DOMs with high quantum efficiency PMTs. There are 50 DOMs spaced 7.5 m apart below the primary dust layer of the IceCube detector. The remaining 10 DOMs are above the dust layer with 10 m PMT spacing. The 78 strings of IceCube surrounding DC are used to reject background events and thereby obtain clean samples of neutrino induced low energy cascade and muon events.

III.3 General Scientific Scope of IceCube

High-energy neutrino astrophysics with IceCube creates a new approach to space and back into time to the highest energy processes in the universe. IceCube can investigate the sources that power active galactic nuclei, the nature of gamma-ray bursts and the origin of the highest energy cosmic-rays. The size of the detector required to probe for astrophysical neutrino sources with reasonable sensitivity can be estimated from the rates of high-energy gamma-rays from various astrophysical sources and the rate of high-energy cosmic-ray protons. For processes with a hadronic origin both charged and neutral pions are produced at comparable rates and these decay to neutrinos and gamma-rays respectively, thereby providing a connection between gamma-ray rates and expected neutrino rates. The cubic kilometer size of IceCube was based on such considerations. IceCube may be able to distinguish between hadronic and radiative sources for interesting objects such as SN remnants and active galactic nuclei since radiative sources would produce few neutrinos. On the other hand, neutrino rates may be enhanced relative to gamma ray rates for dense sources with strong gamma ray absorption. IceCube is performing a general search for point sources of high energy neutrinos in the north sky similar to the search performed by AMANDA [18], with much greater sensitivity. It will also look at particularly promising objects

such as the Crab Nebula and various blazers, micro quasars and x-ray binaries. IceCube can also search for a potential diffuse source of neutrinos associated with the observed diffuse extra galactic x-ray radiation. IceCube can also detect a large burst of low energy neutrinos from a SN explosion or other source such as the birth of an extragalactic black hole. IceCube also has the potential of making significant contributions to particle physics. The lightest super particle in supersymmetric models, generally assumed to be the neutrino, is a prime candidate for cold dark matter. IceCube can perform indirect searches for neutrino or other WIMP particles that are complementary to direct searches performed with cryogenic detectors and by experiments at the LHC. In particular, IceCube is sensitive to neutrino masses above 0.5 TeV that are not accessible at the LHC. IceCube also offers various possibilities for investigating neutrino oscillations with neutrinos from astrophysical sources that travel over enormously long baselines.

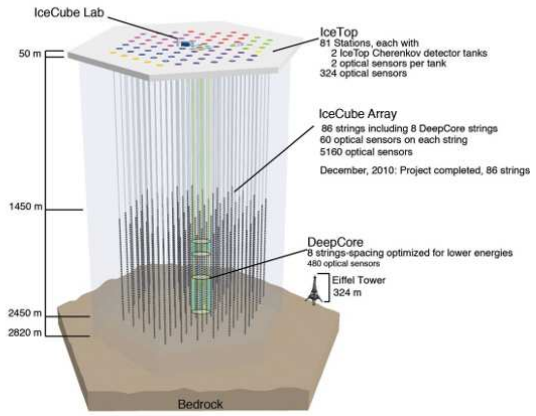

Figure III.1: Schematic drawing of IceCube including the DeepCore. The Eiffel Tower is shaown as a reference for its size.

Figure III.2: Sensor descends down a hole in the ice as part of the final season of IceCube deployment

III.4 DOMs

With previous experience of PMTs in AMANDA, DOMs were designed and used in the IceCube Project. The DOM is the fundamental detector element of IceCube. The devices are built to meet the requirements for good timing, high resolution and durability. Due to the sheer size of IceCube, DOMs are, on average, about 2 km away from the counting house and such long distance causes the broadening of analog signal that could introduce problems. This issue was resolved by digitalizing the signals captured from PMTs. Accordingly, the resolution of photon arrival time is improved to a higher level of few ns, which exceeds that of AMANDA considerably as it only achieved 10 ns timing resolution. Once deployed in the ice, it is impossible to replace dead or problem DOMs, therefore DOMs are rigorously tested before installation. The DOM Structure is illustrated in Fig. III.3 When traveling through the glass shell, a photon hits the PMT and thereby producing photo-electrons (PEs). The signal is then amplified, digitalized, and read out. Finally the signal is time stamped and sent to the surface and the trigger is formed based on such

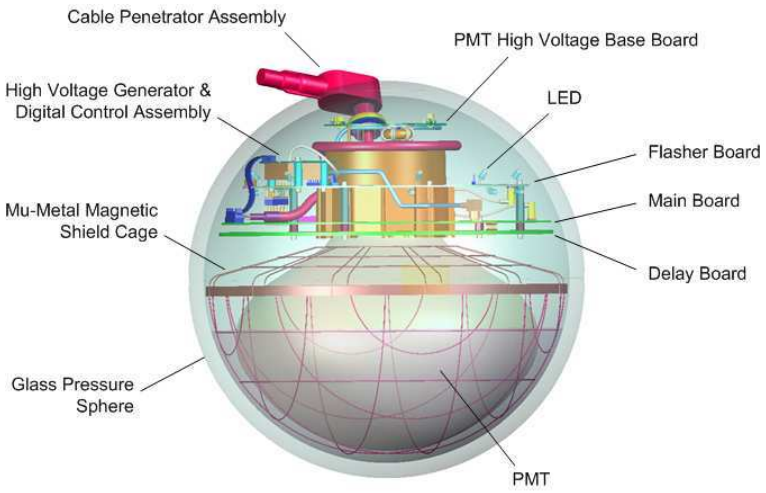

Figure III.3: Schematic cross section of a DOM

time-location information of hits. Each DOM, consists of a 25 cm diameter Hamamatsu R7081-02 PMT and a suite of electronics board assemblies within a 35.6 cm diameter glass pressure housing. Most of the electronics reside on the Main Board (MB), which holds the analog front-end and two analog-to-digital converter (ADC) systems. The digital functions on the MB are performed by a 400K-gate Field Programmable Gate Array (FPGA) containing a 32-bit ARM CPU, 8 MB flash storage, and 32 MB random access memory (RAM). Besides a small built-in real-time operating system (RTOS), the operating parameters of the DOM, FPGA code, and ARM software are all remotely reconfigurable. Timing on the MB is controlled by a nominal 20 MHz quartz oscillator, which is doubled to 40 MHz [20].

Data acquisition is initiated when the PMT signal exceeds 0.3 photo-electrons (PE) for DOMs. The trigger initiates capture and acquisition from 40 Mega Samples Per Second (MSPS) ADC and Analog Transient Waveform Digitizer (ATWD), respectively. A 75 ns delayed signal is set to capture the entire waveform in ATWD. It splits in a dedicated 4-channel circuit board, which covers the entire dynamic range of the PMT, as well as serving calibration and monitoring purposes.

A second board, carrying 12 Lights Emitting Diodes (LED), is also enclosed in the DOM for calibration and verification. Six LEDs are horizontally deployed outward, while the other half are kept 45 degrees upwards.

III.5 Local Coincidence and Calibration

To reduce atmospheric muon cascade backgrounds, IceCube only deals with coincidence events, or 2-DOM hits[22]. There are two types of coincidence, hard local coincidence (HLC), that requires at least one nearest neighboring or next nearest neighboring DOM receive a hit in a time bin of ± 1000 ns; and soft local coincidence (SLC), in which non-neighboring 2-DOM hits are allowed. In SLC mode a DOM stores a compressed digitization header, called charge stamps which are obtained from the three Fast Analog-to-Digital Converters (FADC) samples out of the first 16 samples after the trigger: the highest sample and its two neighboring samples. Although DOM noise rate is a factor of 50 higher in SLC mode than in HLC mode, with current software cleaning algorithms, SLC hits from physics interactions can still be identified with over 90% purity. The addition of SLC allows better detection and analysis at low energies where fraction of SLC hits is large compared with HLC hits. The SLC mode was not available until the 2009 season, before that only HLC mode was in operation. The work started since the deployment of IceCube String-59, the SLC data collection was initialized accordingly . With the last DOM finished in December 2010, the SLC is fully operational now. This analysis uses data from IceCube String-79, as it contains complete SLC hit statistics.

Calibration is the synchronization process between a DOM time and absolute time. after sent out from the surface, the signal is transmitted through DOM IC circuit and results in electrical signal which is resembling with Photoelectric effect.

Pulse is digitalized in the DOM, then the DOM generates the identical analog pulse as original and sends it back to the surface. A DOM readout card deployed on the surface follow the same processes and keeps track of signal time bins and waveforms. Comparison is made every two seconds between two waveforms in order to correct time offset. The waveform bares high precision as 1 ns, thanks to the reliable oscillator on the main board. IceCube DOM locations are also calibrated. During stage 1, the DOM locations are measured multiple times before and after the deployment. and further refined through analysis of Flasher Board Light Emitting Diode (FBLED) data. The total accuracy in position measurement is 50 cm or so, which also means 1.5 ns error in the timing of each readout.

III.6 DeepCore in Detail

Deployment of DC begin in 2008/2009 austral summer. Later 5 more DC strings were deployed with 72 m inter-string spacing in the 2009/2010 season. The construction of DC ended when the last two strings were added, with a even shorter 42m inter-string spacing. The DCe is located at the bottom center of the IceCube detector, the 8 strings therein occupy a cylindrical volume, with a diameter of 250 m and a height of 350 m (shown in Fig.III.4). PMTs in the DC strings were updated with 35 % increase in quantum efficiency compared standard IceCube PMT units, thus help trigger on neutrinos with energies as low as 10 GeV.

To achieve this goal, measures taken are as follows: (1) strings in the DC are more densely placed, with 72 m inter-string spacing compared with 150 m of other strings; (2) on each string, spacing between two adjacent DOMs is reduced from 17 m to 7 m; (3) high quantum efficiency PMTs are implemented, with a 35 % increase in light collection compared with regular IceCube PMT units. These efforts enable the DC to hold 5 times effective photocathode density, thereby enhancing the

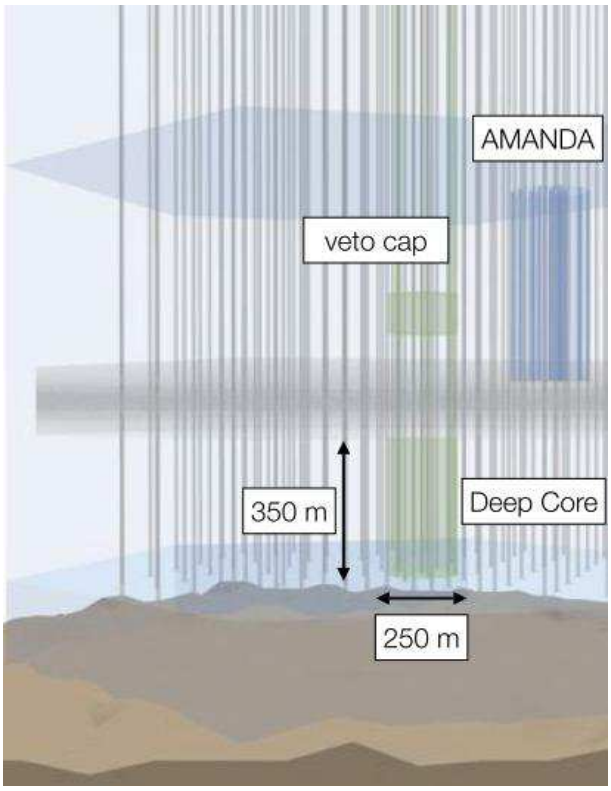

Figure III.4: Schematic view of the DeepCore

capability to detect low energy down-going neutrinos. In the DC, top/outer IceCube DOMs are used to veto atmospheric muons, hence the reduced atmospheric muon entering DC is identified, enhancing the dropped muon detection efficiency in DC volume. With all these efforts, the DC is able to response neutrinos with energies as low as 10 GeV.[21]

III.7 Trigger and Filter

The IceCube SN trigger is designed based on an increase in scalar counts above the dark rates of the PMTs. There are 5160 PMTs in the IceCube and the average noise rate, including the atmospheric muons, is about 280 Hz per PMT. This would introduce a fluctuation of approximately ± 1200. To date, four different trigger gates

have been set, as 0.5 s, 1.5s, 4.0s and 10.0s, respectively. IceCube is designed to report events when significance $\geq 6\sigma$.

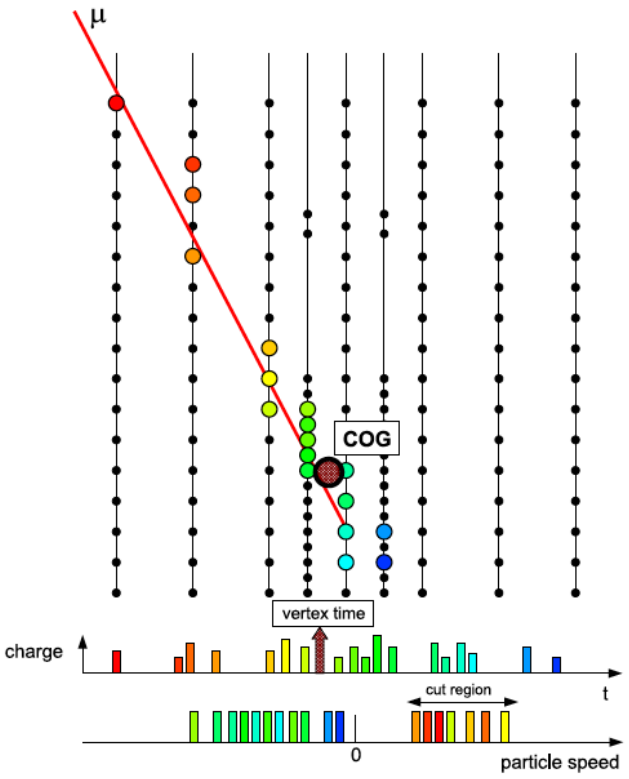

Figure III.5: Structure of On-line Filter System for DeepCore

To reduce atmospheric muon cascade backgrounds, IceCube only deals with coincidence events, or 2-DOM hits[22]. There are two types of coincidence, hard local coincidence (HLC), that requires at least one nearest neighboring or next nearest neighboring DOM receive at hit in a time bin of ± 1000 ns; and soft local coincidence (SLC), in which non-neighboring 2-DOM hits are allowed. In SLC mode a DOM stores a compressed digitization header, called charge stamps which are obtained from the three FADC (Fast Analog-to-Digital Converter) samples out of the first 16 samples after the trigger: the highest sample and its two neighboring samples. Although DOM noise rate is a factor of 50 higher in SLC mode than in

HLC mode, with current software cleaning algorithms, SLC hits from physics interactions can still be identified with over 90 % purity. The addition of SLC information is crucial as it improves event reconstruction, background rejection, and particle identification especially for low multiplicity events. The SLC mode was not available until the 2009 season, before that only HLC mode was in operation. The work started since the deployment of IceCube String-59, the SLC data collection was initialized accordingly . With the last DOM finished in December 2010, the SLC is fully operational now. This analysis uses data from IceCube String-79, as it contains complete SLC hit statistics.

IC-79 was in operation from May 31, 2010 to May 13, 2011. The DC SMT3 triggered at a rate of 185 Hz, which is reduced to 18 Hz through on-line filtering system showed in Fig.III.5 . An event is eliminated if at least one hit in the veto is consistent with v $\sim$ c muon travel speed to the interaction vertex. As a result, 90 % of trigger background is rejected while over 99 % atmospheric neutrinos that interact in the fiducial volume are kept.[22]

CHAPTER IV

EXPERIMENTAL ANALYSIS AND RESULTS

The observation of high energy neutrinos from solar activities associated with the appearance of sunspots and increase in solar flux would establish a third category of astrophysical neutrinos other than ordinary solar neutrinos due to fusion and neutrinos from supernova (SN) 1987A. In this thesis, we show that the frequent SN triggers observed in the IceCube detector and their increasing rate are in fact consistent with neutrinos from solar activities associated with the increase in sunspot formation and their density fluctuations due to the 11-year solar cycle. Sunspots are dark areas formed on the surface of the Sun and may extend deep into its interior with a strong magnetic field. Sunspots are usually correlated with increase in solar flux and are followed by an increase in solar flares and corona mass ejections. In this high magnetic field environment proton acceleration above 100 MeV is common and pion production and subsequent neutrinos from pion and muon decays at much higher energies are possible [5]. We describe an analysis of the existing IceCube data which are consistent with high energy neutrinos ($E_{\nu_e} > 100MeV$) interacting primarily on ^{16}O nuclei in the ice. With the IceCube data we set a flux of $> 5000\nu_e(\bar{\nu}_e)/cm^2.s$ on Earth.

We studied solar activities due to the increase in the number of sunspots and the IceCube SN trigger rate. The results are shown in figure IV.10 where the top plot shows the solar sunspot rate obtained from the National Geophysical Data Center (NGDC) [30] and the bottom plot is the IceCube SN trigger rate over the

past two and a half years.Comparison of the two plots clearly shows correlation between the number of sunspots and the IceCube SN trigger rate for solar cycles 23 and 24. Note, the majority of the SN triggers in the IceCube data only last 0.5 seconds. The data in figure IV.10 clearly show a high degree of correlation with the increasing density of sunspots.

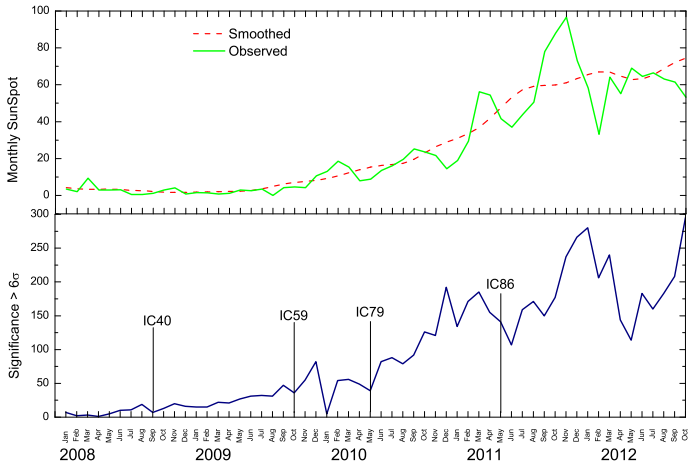

Figure IV.1: The sunspot activities of the Sun over the past 3.8 years. The dashed line represent the average value (top). The IceCube SN trigger frequency for the same time period (bottom).

We also studied the rate of x-ray emissions from the sun for the months of January through May 2011, obtained from the GOES-15 satellite [30], and the trigger rate for the SN triggers in the same time period. This comparison is shown in figure IV.2. There is a clear clustering of events occurring in certain time periods indicating a definite correlation between the two datasets.

The SN trigger is designed for a 0.5, 4.0 and 10.0 s interval with an overall rise of the scalars at least 6σ above the fluctuation of DOM dark rates plus the average atmospheric muon hits. Figure IV.10, bottom plot, shows the trend of these triggers

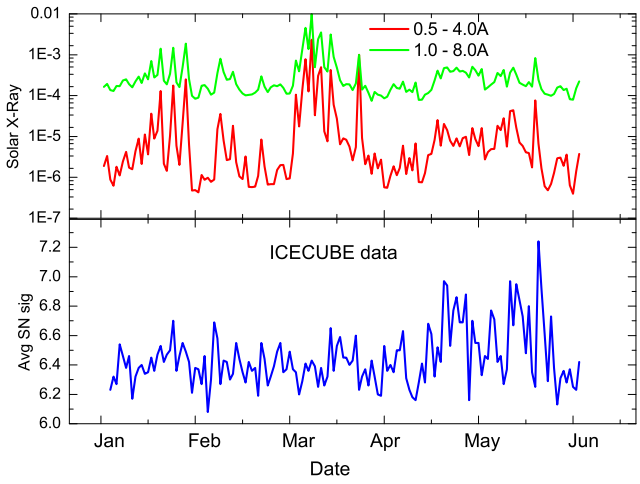

Figure IV.2: The x-ray emission activities of the Sun over the months of January through May 2011 (top plot). The IceCube SN trigger frequency for the same time period (bottom plot).

logged from September of 2008 through September of 2012. These two plots reveal a striking resemblance and we expect the IceCube SN trigger rate to increase as the solar cycle number 24 reaches its maximum in 2013.

In order to calculate the expected rates of these high energy neutrinos ($100MeV$), the flare neutrino spectrum of Fargion and Di Giacomo [5], shown in figure (solid circles) IV.3, was parametrized above a neutrino energy of 80 MeV (solid line). This parametrized form is shown in the following equation.

$$\frac{dF}{dE} = (110 \pm 20)x^{-0.41\pm0.10}(1+x)^{-4.5\pm0.2} \tag{IV.1}$$

In the above equation $x = \frac{E}{1000MeV}$, where E is the neutrino energy in MeV. The fit $\xi^2 = 0.38$ and $\Delta F = \pm 10\%$.

In figure IV.3, limits set on solar flare neutrinos from Baksan and Kamiokande II are also shown.[16]

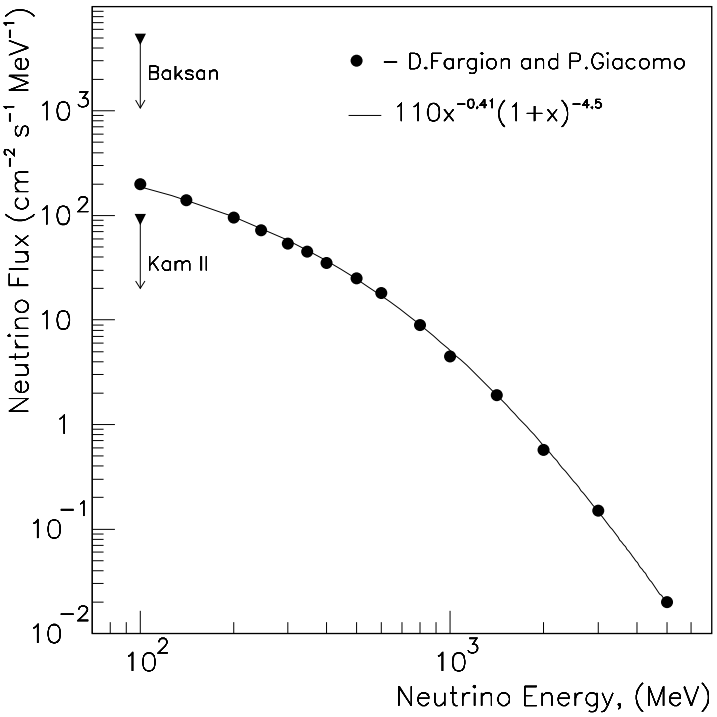

Figure IV.3: The neutrino energy spectrum of reference [5] (points) and the its parametrized form (line).

The dominant interactions in the IceCube detector are

$\nu_e + ^{16}O \rightarrow e^- + p + X$, $\bar{\nu}_e + ^{16}O \rightarrow e^+ + n + X$ and $\bar{\nu}_e + p \rightarrow e^+ + n$.

Using the above parametrized neutrino flux, the flux-averaged cross sections for these reactions are estimated to be $(4.0 \pm 1.0)\times 10^{-38} cm^2$, $(1.0 \pm 0.2)\times 10^{-38} cm^2$ and $(0.4 \pm 0.1)\times 10^{-38} cm^2$, respectively, from a Fermi-Gas model (FGM) of Gaisser and O'Connell [23]. The estimated errors are obtained from the uncertainties for the FGM calculations quoted by Vogel [25].

The simulated 3-momenta of these events for electrons were written to a file which was then read by the Geant/GCALOR MC code and muon transport was simulated. The interaction vertices were distributed uniformly throughout the detector volume. The Geant Cherenkov code together with the input IceCube

geometry with average DOM quantum efficiency as well as an ice model with appropriate absorption and scattering simulated the hit DOMs. The resulting trigger efficiency for the number of hit DOMs ≥ 1 is $\approx 0.15\%$. Figure IV.4 shows the input muon neutrino energy spectrum (top) and the muon spectrum (bottom)

The muon energy spectrum from the input neutrino energy spectrum of figure IV.3 is shown in figure IV.5. To obtain the total noise for the same 0.5-second time interval of all 5060 operating DOMs, we multiply the number of DOMs by the time $\Delta t = 0.5$ seconds and the dark rate plus average atmospheric muons of 280 Hz, therefore,

$$DetectorNoise = 5060 \times 280 \times 0.5 = 708400 \tag{IV.2}$$

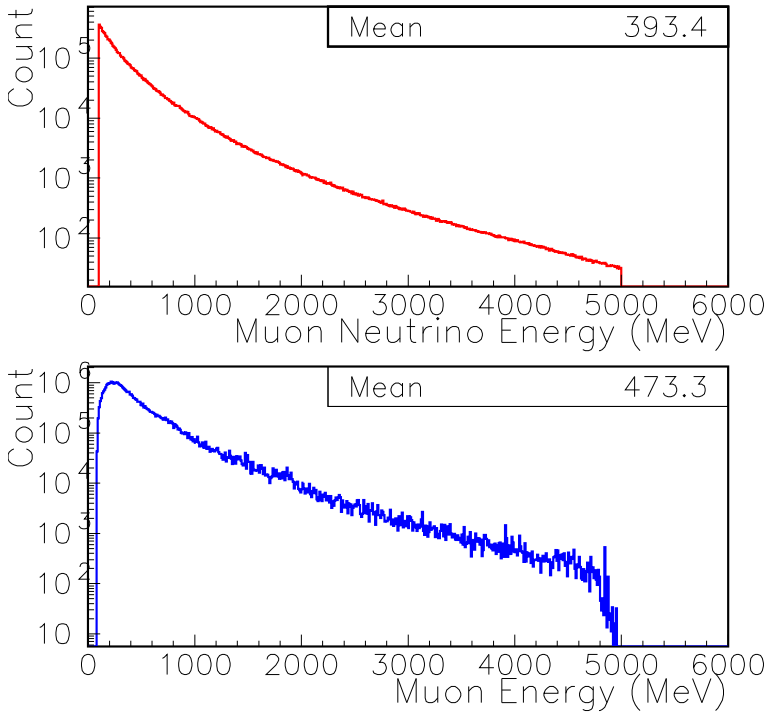

Figure IV.4: The input muon neutrino energy spectrum and the muon spectrum

This value gives rise to a statistical fluctuation of σ equal to $\pm \approx 840$ in a 0.5-s

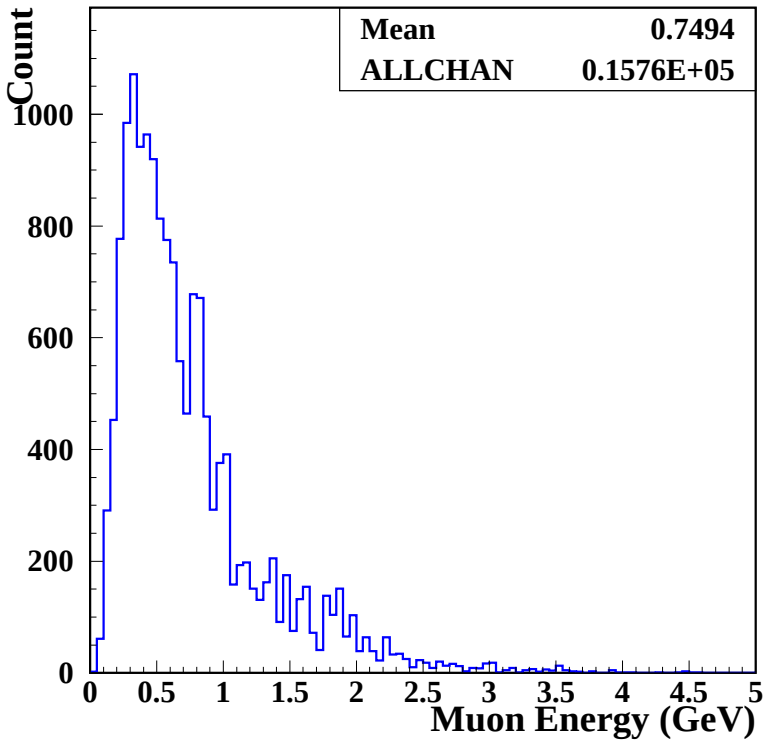

Figure IV.5: The energy distribution of the muons triggering at least one DOM.

interval. With a SN trigger of $\geq 6\sigma$, we estimate 5000 hits per 0.5 s, or $> 2550/s$ we, therefore, expect a neutrino shower of $5000/cm^2.s$ at the South Pole. We quantify this rate with the following calculations. The lower limit of the neutrino flux due to solar flares is calculated using the values for the neutrino reaction cross section $(4.0 \pm 1.0) \times 10^{-38} cm^2$), a 6σ signal of 2550 hits, the total number of target ^{16}O atoms $4.20 \times 10^{37} \pm .01$, and the overall efficiency of $0.15 \pm .05$.

$$Flux \geq 5000 \pm 1250/cm^2.s \tag{IV.3}$$

Note, this limit is only achievable with the IceCube detector. As shown in figure IV.3 this observation is above the SK sensitivity.

The Fermi-LAT collaboration [29] has recently reported that during the Coronal Mass Ejection (CME) M3.7, a significant number of high energy

($E \geq 100MeV$) γ-rays were detected from the Sun after the impulsive phase of M3.7 flare on 7 March, 2011.

We also note that during this event (M3.7) there was abnormally high rate of SN triggers in the IceCube detector.

During the March 6 to March 8, 2011 time period, the SN triggers above 6 σ recorded were 31. The SN triggers are recorded for 0.5, 4.0 and 10.0 second intervals and are not event-by-event triggers. They record an overall rise in scalar counts for all of the DOMs in the IceCube.

It is noteworthy that the Super-K detector with a fiducial volume of 22 k-tons would detect less than 0.003 events during the same time window of 0.5 seconds. For this estimate we assumed a detection efficiency of 0.023, for the SK detector[2].

IV.1 Introduction to Significance Level

Statistics significance describes the likelihood of a specific cause, with certain degree of error. The level at which one can accept whether an event is statistically significant is known as the significance level or p-value, it is usually denoted by the Greek symbol α. In fields like nuclear and particle physics, the it is common to express significance level in the unit of standard deviation σ. The statistical significance of $n\sigma$ can be converted into a value of α via the use of error function;

$$\alpha = 1 - erf(n/\sqrt{2}) \tag{IV.4}$$

Where erf is the error function, and it is defined as:

$$erf(x) = \frac{2}{\sqrt{\pi}} \int_0^x e^{-t^2} \mathrm{dt} \tag{IV.5}$$

Table 2: Standard deviation and fluctuation

Sigma	Percentage	fluctuation
1	68.2689492 %	1/3.15
2	95.4499736 %	1/22
3	99.7300204 %	1/370
4	99.993666 %	1/15800
5	99.9999426697 %	1/1740000
6	99.9999998027 %	1/507 000 000

If a data distribution is approximately normal then about 68% of the data values are within one standard deviation of the mean (mathematically, $\mu \pm \sigma$, where μ is the arithmetic mean). A more detailed information of standard deviation and percentage is tabulated in 2.

In this thesis, we analyzed $\geq 6\sigma$ result, i.e. there's a 1 in 507 million chance that it was the result of a statistical fluctuations over the range of total SN trigger events. This is under the assumption that no other background aside from the above mentioned DOM noise and atmospheric muons is at work.

IV.2 Estimation of High Energy Solar Neutrino Flux

In this section, we describe in detail how the flux high energy solar neutrinos (100MeV) is evaluated. The muon and electron neutrinos appear to be dominant against atmospheric neutrino background at above 80 MeV in neutrino spectrum plot in figure IV.6 from the work done by Fargion and Moscato.[24]

The dominant interactions in the IceCube detectors are

$$\nu_{\mu,(e^-)} + O^{16} \rightarrow \mu^-, (e^-) + p + X \tag{IV.6}$$

$$\bar{\nu_{\mu,(e^+)}} + O^{16} \rightarrow \mu^+(e^+) + n + X \tag{IV.7}$$

$$\nu_{\mu,(e^+)}^{-} + p \rightarrow \mu^+(e^+) + n \tag{IV.8}$$

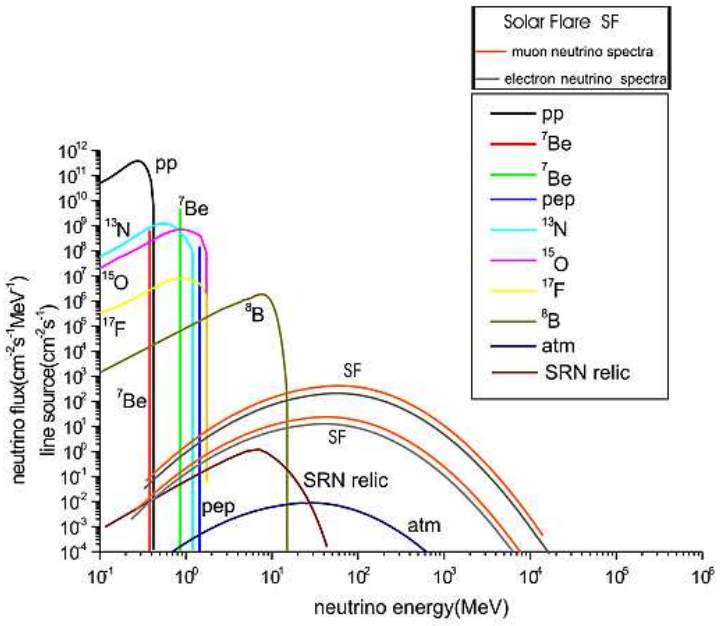

Figure IV.6: Solar neutrino Flare fluxes over the known atmospheric neutrino background. The primary solar flare spectrum is considered as the atmospheric one at least within the energy threshold E $\simeq$ 100 MeV up to 10 GeV above the atmospheric noise.

The flare neutrino spectrum over 80 MeV can be parametrized by the following equation, where $x = \frac{E}{1000MeV}$, E is the neutrino energy in MeV. In this thesis, we only simulated $\nu_{\mu,(e^-)} + O^{16} \rightarrow \mu^-, (e^-) + p + X$

$$\frac{dF}{dE} = (110 \pm 20)x^{-0.41\pm0.10}(1+x)^{-4.5\pm0.2} \tag{IV.9}$$

As shown in figure IV.7 the majority of the triggers are single hits in the IceCube detector. with a SN trigger of $\geq 6\sigma$, we expect 2550 hits per 0.5 second, or a neutrino shower of $5000/cm^2.s$ at the South Pole. To calculate the lower limit of solar neutrino flux, the values used are as the following: the neutrino reaction cross

section ($(4.0 \pm 1.0) \times 10{-}38 cm^2$), a 6σ signal of 2550 hits, the total number of target O^{16} atoms $4.20 \times 10^{37} \pm .01$ and the overall efficiency of $0.15 \pm .05$.

$$Flux \geq 5000 \pm 1250/cm^2.s \tag{IV.10}$$

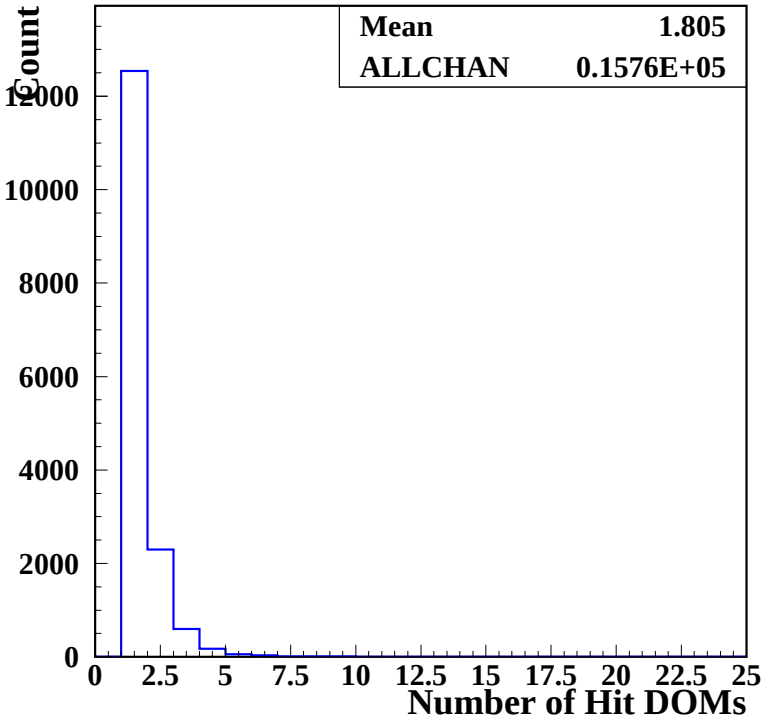

Figure IV.7: Number of hit DOMs in the IceCube detector due to muons produced via the CC interactions of $\nu_\mu + ^{16} O \rightarrow \mu + X$.

We must emphasize that this is approximately half the flux calculated by Fargion and Moscato.[24]

IV.3 Supernovae Trigger and Sunspot Correlation

In order to find the correlation between solar and SN activities, we analyzed SN trigger rates, and a variety of solar activities such as sunspot number, radio flux 10.7cm, proton flux, X-ray.

Table 3: Observed monthly sunspot number.

Year	Jan	Feb	Mar	Apr	May	Jun	Jul	Aug	Sep	Oct	Nov	Dec
2008	3.4	2.1	9.3	2.9	2.9	3.1	0.5	0.5	1.1	2.9	4.1	0.8
2009	1.5	1.4	0.7	1.2	2.9	2.6	3.5	0.0	4.2	4.6	4.2	10.6
2010	13.1	18.6	15.4	7.9	8.8	13.5	16.1	19.6	25.2	23.5	21.6	14.5
2011	19.0	29.4	56.2	54.4	41.6	37.0	43.9	50.6	78.0	88.0	96.7	73.0
2012	58.3	33.1	64.2	55.2	69.0	64.5	66.5	63.1	61.5			

Table 4: Predicted monthly sunspot number.

Year	Jan	Feb	Mar	Apr	May	Jun	Jul	Aug	Sep	Oct	Nov	Dec
2008	4.2	3.6	3.3	3.3	3.5	3.2	2.7	2.6	2.2	1.8	1.7	1.7
2009	1.8	1.9	2.0	2.2	2.3	2.7	3.6	4.8	6.1	7.0	7.5	8.2
2010	9.2	10.6	12.3	13.9	15.4	16.3	16.7	17.4	19.6	23.2	26.5	28.9
2011	31.0	33.5	36.9	41.8	47.6	53.2	57.3	59.1	59.6	59.9	61.1	63.4
2012	65.5	66.9	66.8	66.1	65.7	66.2	68.2	71.8	75.1	77.4	79.4	80.9

To make the results uniform with the earlier data in SN trigger events, we filtered out the triggers within 1.5 second time bin, which was added to the statistics in Jan 2012. Before that only data of 0.5s, 4s, and 10s time bins were available. In addition, to make sure the triggers are not coherent, we eliminated lower one in the two triggers within 20 minutes. As for the observed and predicted sunspot numbers, we obtained the data from the IPS Radio and Space Services in Bureau of Meteorology, Australia[26]. The data was selected from 2008 to 2012, as shown in table 3 and 4.

The results are displayed in figure IV.8, at the top is sunspot rate obtained from the National Geophysical Data Center (NGDC) and the plot below is the IceCube SN trigger rate over the past three and a half years.

The time span is from 2008 to present, which contains the end of solar cycle 23

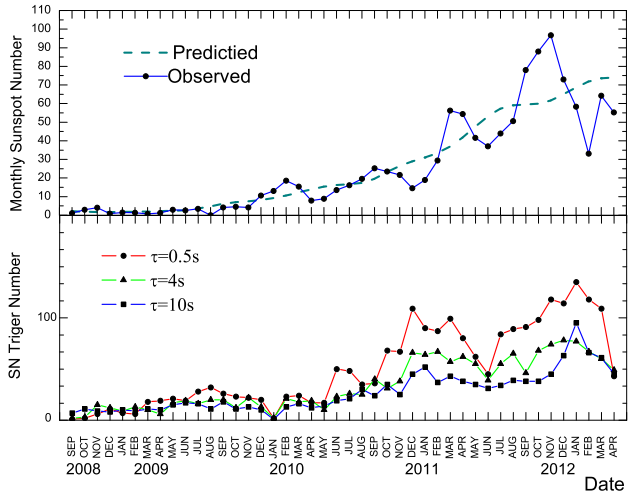

Figure IV.8: The sunspot activities of the Sun over the past 3.6 years. The dashed line represents the smoothed expectation value (top). The IceCube SN Trigger frequency during the same period(bottom). Note that to date, the 0.5 triggers are dominant, accounting for about half of the total triggers. The 0.5 trigger frequency closely resembles the density of sunspots.

and first quarter of solar cycle 24, the sunspot number plot demonstrates an obvious increasing trend. In the lower plot, 0.5 second triggers are dominant, which means that large numbers of SN triggers lasts no longer than half second. These data, especially the regression line in figure IV.9 show the noticeable degree of consistency with the increasing number of sunspots.

To better determine the consistency of data, we examined the correlation coefficient. The correlation coefficient, denoted by r, is a measure of the strength of the straight-line or linear relationship between two variables. The range of r is between -1 and 1. If the value is zero, it means there is no linear relationship between the two variables. Values between 0 and 0.3 (0 and -0.3) indicate a weak positive (negative) linear relationship via a shaky linear rule. Values between 0.3 and 0.7 (-0.3 and -0.7) indicate a moderate positive (negative) linear relationship

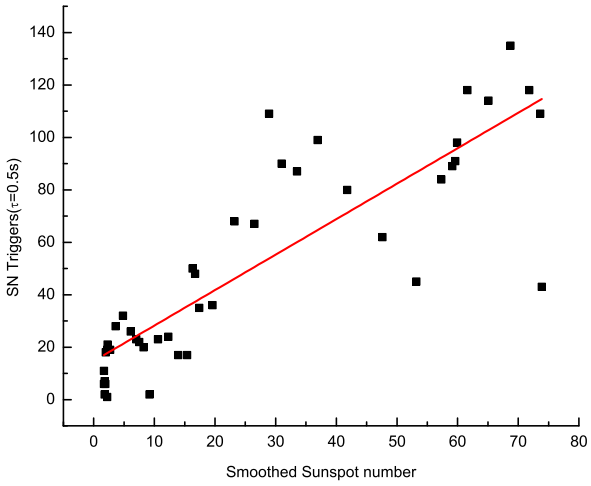

Figure IV.9: The linear regression of smoothed(predicted) sunspot number and IceCube SN trigger at 0.5 second bin.

via a fuzzy-firm linear rule. Values between 0.7 and 1.0 (-0.7 and -1.0) indicate a strong positive (negative) linear relationship via a firm linear rule. The most familiar measure of correlation coefficient is the Pearson product-moment correlation coefficient, or "Pearson's correlation", it can be written as the IV.12.

$$corr(X,Y) = \frac{cov(X,Y}{\sigma_X \sigma_Y} \quad \text{(IV.11)}$$

$$= \frac{E\left[(X-\mu_X)(Y-\mu_Y)\right]}{\sigma_X \sigma_Y} \quad \text{(IV.12)}$$

For a series of n measurements of X and Y, the correlation coefficient is written as IV.14, where $\bar{x}$ and $\bar{y}$ are the sample means of X and Y, and σ_X and σ_y are the sample standard deviations of X and Y.

$$r_{xy} = \frac{\sum_{i=1}^{n}(x_i-\bar{x})(y_i-\bar{y})}{(n-1)\sigma_x \sigma_y} \quad \text{(IV.13)}$$

$$= \frac{\sum_{i=1}^{n}(x_i - \bar{x})(y_i - \bar{y})}{\sqrt{\sum_{i=1}^{n}(x_i - \bar{x})^2 \sum_{i=1}^{n}(y_i - \bar{y})}} \quad \text{(IV.14)}$$

In this work, Microsoft Excel 2007 is used to calculate the correlation coefficient between monthly sunspots and SN trigger events. The result is 0.7882, which is considered to be a strong positive linear relationship. The same method is also applied to the compilation of random events, that we compare the entire actual SN trigger events and random events generated by computer, the result is -0.0619, in other words, at least 93.8% of the SN trigger events are considered as invalid candidates.

The SN trigger is designed for a ten-second interval with an overall rise of the scalars at at least 6σ above the fluctuation of the DOM dark rates. The bottom plot in figure IV.8 shows the trend of those triggers logged from September 2008 through this date. The comparison of the two plots indicates a high degree of correlation and we anticipate the IceCube SN trigger rate to raise as the solar cycle 24 reaches the peak in 2013.

To better compare the IceCube SN data with the Solar sunspot correlation, we narrowed the time range to January through May, 2012. As illustrated in figure IV.10, the comparison of Sunspots plot at the top and the IceCube SN average significance at the bottom yields a correlation to a much better degree of precision.

IV.4 Supernovae Trigger and Other Solar Data

Solar radio flux is also investigated in this thesis, as it is a significant indicator of overall solar activity levels. We analyzed the 10.7 cm flux data, which is near the peak of observed solar radio emission. The data was retrieved from January through May 2012, from satellite GOES-15 [30]. For comparison, we also display SN trigger during the same period, as shown in figure IV.11. There is a clear clustering of events occurring in certain time periods indicating a definite correlation between the

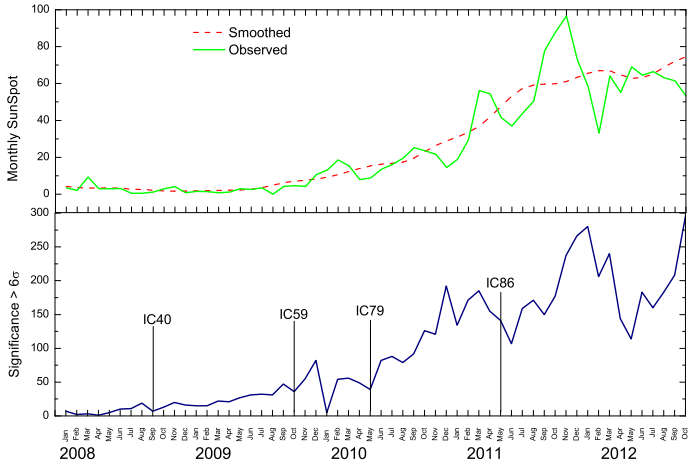

Figure IV.10: The observed sunspot numbers over the months of January through May 2012 (top plot). The IceCube SN Trigger daily average significance ($\sigma > 6$) during the same period(bottom).

two datasets.

From comparison of the two plots above, it is clear that the solar radio flux 10.7 cm intensity and the average SN trigger significance are closely related. Notice that the trend of the two plots are highly consistent after January. These data in figure IV.11 clearly show correlation with the fluctuation of solar radio flux.

Strong x-rays are emitted from the solar corona, which is the upper layer of the Sun's atmosphere. In this thesis, Solar x-ray flux data are obtained from Satellite GOES15, and we analyzed the 5 minute data, with the x-ray wavelength of 0.5-4.0 Åand 1.0-8.0 Å. We eliminated the negative x-ray flux data, as it may be due to flux overflow or system errors. As both the short (0.5 - 4.0 Å) and long (1.0-8.0 Å) solar X-ray data have a very wide range, we take the logarithm so that the results can be compared more conveniently.

As shown in figure IV.12the IceCube data and Solar x-ray long wavelength (1.0 - 8.0 Å) plot show correlation to a certain degree. However, the peak appears in

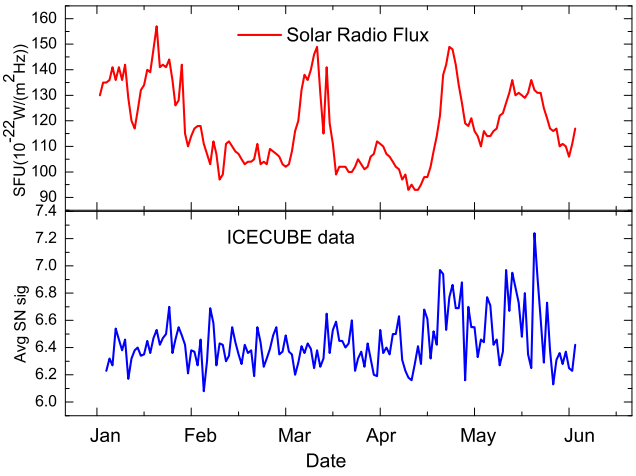

Figure IV.11: The Solar Radio Flux 10.7cm over the months of January through May 2012 (top). The IceCube SN Trigger average Significance ($\sigma > 6$) during the same period (bottom)

the IceCube data in May while the solar X-ray flux remain comparatively less active. In addition, it can be observed that the Solar x-ray flux data, both the long and short wavelengths, reach the peak in early March, with 2.33×10^{-3} and 9.81×10^{-3}, respectively. The correlation suggests a possibility that the IceCube SN trigger may be in in response to Solar x-ray flux, but the time range doesn't fit for the same period.

The IceCube SN trigger frequency, on the other hand, fits better with the Solar x-ray Flux, as shown in figure IV.13 for most of the months during January through May 2012, with the exception of the mid April to mid May in which the Solar x-ray flux (long wavelength) appears flat and the short wavelength x-ray flux gives a small upwards bump; meanwhile, the corresponding SN IceCube trigger frequency plot has a trough during the same time period. On the rest of the plots, it can be observed that the two peaks appear during around the same time period, which shows a consistency to a considerable degree. There is a slight different in the

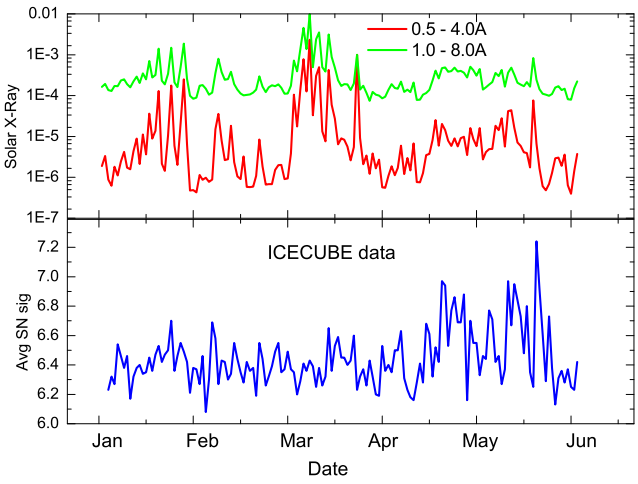

Figure IV.12: The long(1.0 - 8.0 Å) and short(0.5 - 4.0 Å) Solar Xray Flux over the months of January through May 2012 in logarithm (top). The IceCube SN Trigger average Significance ($\sigma > 6$) during the same period (bottom)

magnitude of the peaks. For the Solar x-ray flux data, both short and long wavelength, a larger peak exist during March, in comparison, the SN IceCube frequency is even higher over January than March.

We also investigated the Solar proton events over the period of January through May 2012. We analyzed the proton flux spectra of $> 1MeV$ and $> 10MeV$ [27], and for dominant events during the period, table 5 is listed for better reference.

Comparison between Solar Proton Flux and SN IceCube data, as shown in figure IV.14 indicates the consistency of solar proton activities and IceCube trigger frequency to a high degree. The top plots show exactly the dominant events displayed in table 5, and such events are distributed in January, March and May. For the rest of the period, the curves are relatively flat or inactive, especially for Solar proton flux > 10 MeV. The corresponding SN IceCube data plot demonstrates similar curves, with the exception of April which is comparatively quite in both of the Proton flux plots, while an obvious bump appear in April at the SN IceCube

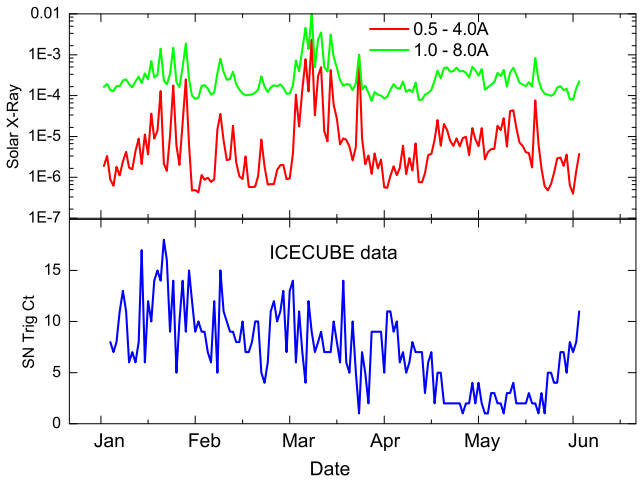

Figure IV.13: The long (1.0 - 8.0 Å) and short (0.5 - 4.0 Å) Solar x-ray Flux over the months of January through May 2012 in log scale (top). The IceCube SN Trigger event frequency during the same period (bottom)

plot.

IV.5 Atmospheric Muon Contribution to the SN Triggers

The significance for the SN triggers, assuming nearly identical DOMs, is obtained from the equation IV.15.

$$significance = \frac{N_T - N_B}{\sqrt{N_B}} \tag{IV.15}$$

In the equation above, N_T is the total number of events, i.e. excess plus background; N_B is the total number background, that is DOM noise plus atmospheric muons. Note, the background due to the atmospheric muons is the average seasonal rate of $700 \pm 26Hz$ for IC-86 as shown in figure IV.15. Therefore, a possible SN excess or any other excess is $Excess = N_T - N_B$.

Table 5: Major Solar Proton Events, Jan 2012 - Present.

PARTICLE EVENT		
Start (Day/UT)	Maximum (Day/UT)	Proton Flux ($> 10MeV$)
$Jan23/0530$	$Jan24/1530$	6310
$Jan27/1905$	$Jan28/0205$	796
$Mar07/0510$	$Mar08/1115$	6530
$Mar13/1810$	$Mar13/2045$	469
$May17/0210$	$Mar17/0430$	255
$May27/0535$	$May27/1045$	14

In order to find the entire detector noise and the contribution of the atmospheric muons for the same 0.5s time interval for the IceCube Detector, we multiply the number of DOMs by the time $\delta = 0.5$ second and the dark rate plus atmospheric muons of 280 Hz, therefore

$$Noise/0.5s = 140 \times 5060 = 708400 \tag{IV.16}$$

Where, 5060 is the number of working DOMs. Thus the total SN Background due to PMT noise and atmospheric muon is;

$$SNBackground = 708400 + 21000 = 729400 \tag{IV.17}$$

Taking the square root of 729400, it gives rise to a statistical fluctuation of σ equal to $\pm \approx 840$ in a 0.5 second time window.

Figure IV.16 show the MC calculations for both the SN raw single hit data and the SMT8 data. Note, the SMT data does not include the usual HLC cut and

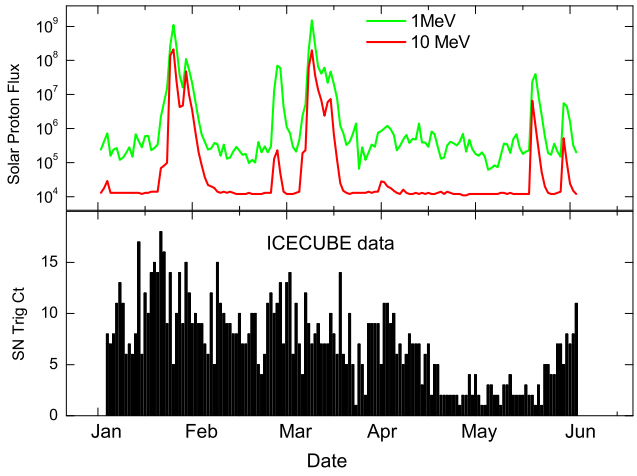

Figure IV.14: The Solar Proton fluxes of over 1 MeV and 10 MeV over the months of January through May 2012 in logarithm (top). The IceCube SN Trigger event frequency during the same period (bottom)

that is why has a lower mean value of 13.5 channels rather than the usual mean of 16 or 17 channels. From figure IV.16 the ratio of the single hits to SMT8 is approximately 6.3. We estimate this ratio would increase to 8 if HLC is applied.

The values for the excess due to different flux of the atmospheric muons are tabulated in 6.

The SN trigger in the IceCube Detector, by design, has a 250 μs dead time. This was implemented so that the dark rate of the PMTs can be decreased to 280 Hz. Considering the total noise is for 0.5 s, $5060 \times 140 = 708400 Hz$, we take the square root and we get the fluctuation of total noise for 1σ event, which is approximately 840 Hz. Note that the fluctuation of muon is just for 7σ fluctuation of the atmospheric muons in only 1774 Hz, which is much smaller compared with the total sensitivity required for $6\sigma = 5040$ event, therefore, the muon contribution to the SN trigger, accordingly, is negligible. Actually, this can be observed from the

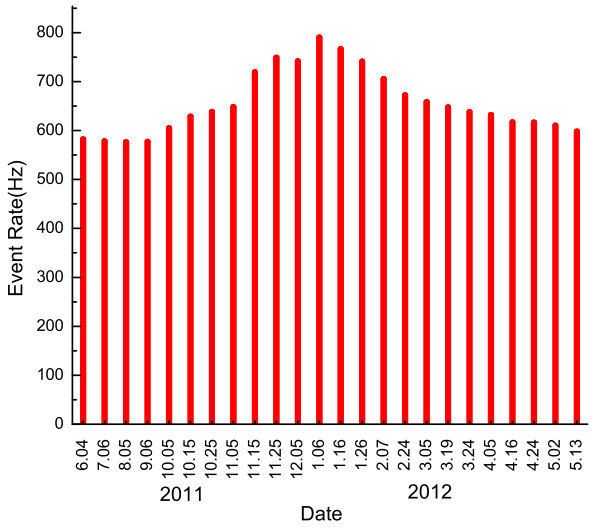

Figure IV.15: The seasonal variation of muons is the IceCube for IC-86. These data are HLC, SMT8 and SMT3 for the IceCube and the DC, respectively.

experimental data, as shown in IV.8, in early 2008 with the IC-40 IceCube configuration, the monthly 6σ SN trigger is almost zero, if the muon did play an important role in the total SN trigger rate, then IC-40 SN trigger rate cannot be zero.

IV.6 Supernovae Trigger and DeepCore SMT3

The DC in IceCube consists of 6 and 8 strings for the IC-79 and the IC-86 configurations, respectively. We looked at the hit-cleaned data where only two DC DOMs fire. According to the muon spectrum of figure IV.7, we believe the SMT3 trigger efficiency for these muons is too low. This allows the detection of higher energy SN neutrinos as the DOMs on these strings are closely mounted, i.e. 7 meters, and the DOMs are also more sensitive, due to higher quantum efficiency PMTs. We analyzed the N-Channel ≤ 3 data retrieved from IC-79 and IC-86. The IC-79 (May 2010 May 2011) data covered 348 days, over 90% of the data are high

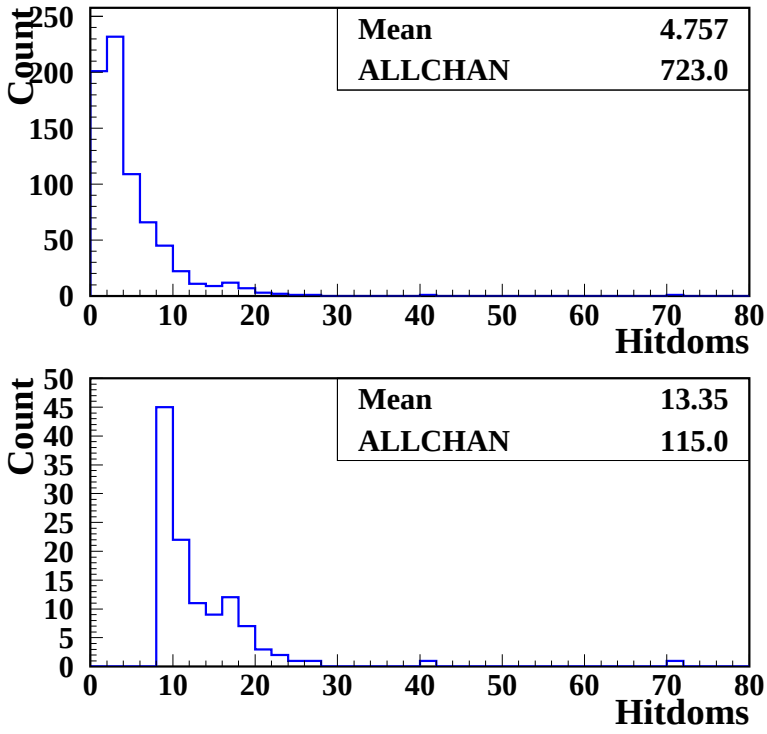

Figure IV.16: The MC N-Channel distributions for the no trigger (top) and the SMT8 trigger (bottom)

quality and used for the analysis. A low threshold trigger (SMT3), requiring 3 or more HLC hits within 2500 ns, is applied to DOMs in DC. The DC on-line filter runs on the SMT3 triggered event sample, with 17.5 Hz pass rate. The filter algorithm starts by calculating the center of gravity (COG) of all HLC hits in the fiducial volume to get an interaction vertex and time estimate. Then the filter disregards any events consistent with a cosmic ray muon entering the detector volume by examining the speed between an individual HLC hit in the veto volume and the COG [28]. A factor of 10 reduction in data compared to the triggered events are reached by this algorithm while keeping 99% atmospheric neutrinos that interact in the fiducial volume. After applying noise cleaning algorithms, events with ≥ 8 remaining hits and ≥ 4 hits in the fiducial region are chosen for later analysis.

The offline pulses were further subjected to the following hit cleaning filters,

Table 6: Signal strength due to different flux of the atmospheric muons

Sigma	Average number of Muons + Signal/0.5s	Expected number of muons DOM hits/0.5s	Excess Hits
Bkg	2800	13440	0
1	2853	13694	254
2	2906	13949	504
3	2959	14203	758
4	3012	14458	1012
5	3065	14712	1266
6	3118	14866	1520
7	3171	15221	1774

which we list verbatim from the website
http://wiki.icecube.wisc.edu/index.php/IC79_offline_processing.

CalibrateAndExtractOffline:

- seeded RT cleaning (R=150 m, T=1000ns, seed=HLC)
- bad DOM cleaning (static IC59 list + db query)
- no first launch cleaning
- HLC/SLC cleaning
- FeatureExtractor (full extraction)
- NFE (default settings, FADC, ATWD, SLC extracted separately, then merged)
- SLCHitExtractor (-10ns fudge to match timing with FE)

The comparison between DC filtered data and IceCube SN trigger frequency, shown in figure IV.17, indicates the DC SMT3 events directly corresponds to the IceCube SN event triggers, as the DC filtered trigger begins to increase significantly

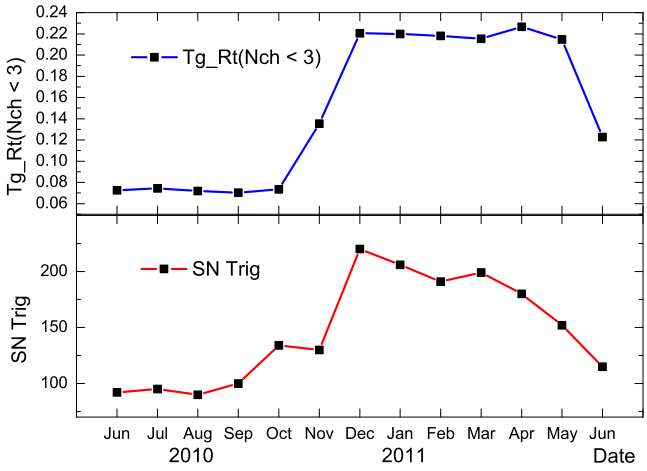

Figure IV.17: The DC SMT3 triggers (top) and the the IceCube SN trigger event frequency during the same period (bottom)

from October to December 2010 and the IceCube SN event, begins to increase from September to December 2010. It can be also observed that, even though finally both plots drop slightly, the DC SMT3 events plot keeps flat from January to May 2011. These activities show a high degree of correlation with the solar activities in the same period. Note, we only used the burn sample for the for this analysis. It is noteworthy, the DC data show the excess must be due neutrino intercation in the IceCube. A full analysis of the DC data, within the method presented in this thesis, is highly recommended.

CHAPTER V

SUMMARY AND CONCLUSIONS

In summary, we have studied the correlation between IceCube SN candidate trigger events and various solar activities, and the DC SMT3 triggers. During the first half of Solar Cycle 24, the monthly sunspot numbers increases as we expect, the IceCube SN trigger events also increase, following almost exactly the same trend. The analysis of recent solar activities since January 2012, including solar x-ray, radio 10.7cm, proton and photon flux, and the IceCube trigger events, indicate an overall correlation to a high degree.

The observed monthly sunspots numbers, as a significant indicator of overall solar activities, reached the peak of 96.7 in November 2011, and drops considerably to a deep trough in February 2012 at 33.1. The monthly IceCube SN trigger event numbers meanwhile, reaches the peak of 280 in January 2011, then declines sharply to the lowest 140 in May 2012. A delay of roughly two months, and similar tendency shows a strong correlation. More recent data, which began in January 2012 to present, demonstrates 3 peaks in late January, early March and Mid-May respectively, in the overall solar activities, and the IceCube SN event triggers behave in the similar manner. The DC SMT3 trigger rate from IC-79 and IC-86, compared with IceCube SN trigger event data, are also show a high degree of correlation.

Solar activities and IceCube Supernova triggers correlation are currently under study by the Southern University group, and would help in the prediction and analysis of IceCube SN event behaviors based upon solar activities in the near

future. Once the existence of high energy solar neutrinos is established, we believe a new window will be opened to the study of neutrino physics, stellar physics as well as cosmological neutrino densities and their role in a new understanding of the universe.

BIBLIOGRAPHY

[1] On the Problem of Detecting Solar Neutrinos (J. N. Bahcall and R. Davis, Jr.), Stellar Evolution (ed. R. F. Stein and A. G. W. Cameron, Plenum Press, N.Y., 1966), pp. 241-243; Solar neutrinos observed by GALLEX at Gran Sasso., Anselmann, P. et al. (GALLEX), Phys. Lett. B285 (1992) 376-389.

[2] Super Kamiokande Collaboration, R. Wendell, et al., arXiv:1002.3471v2, Phys. Rev. D 81, 092004 (2010).

[3] Nuovo Cim., 105A, n.12, 1798, 1992 (Collaborazione LVD)

[4] A.R. Fazely, S.V. Ter-Antonyan and X. Xu, "First Observation of High Energy Solar Neutrinos Correlated with Sunspots in IceCube", Southern University Technical Note, January 30, 2011.

[5] D. Fargion and P. Di Giacomo, Nucl. Phys. B (Proc.Suppl.) 188, (2009) 142.

[6] *http* : *//en.wikipedia.org/wiki/Neutrino*

[7] C.L Cowan Jr., F.Reines, Detection of the Free Neutrino: a Confirmation, Science 124(3212): 103-4(1956).

[8] J. Beringer et al. (Particle Data Group), Phys. Rev. D86, 010001 (2012)

[9] Michael Woolfson ,The origin and evolution of the solar system. Astronomy & Geophysics, Vol41, Issue1, 12-19(February 2000)

[10] Kogut, A. et al., Dipole Anisotropy in the COBE Differential Microwave Radiometers First-Year Sky Maps, Astrophysical Journal. 419: 1 (1993).

[11] *http* : *//en.wikipedia.org/wiki/Standard_solar_model*

[12] John N. Bahcall et al., 10,000 Standard Solar Models: A Monte Carlo Simulation, The Astrophysical Journal Supplement Series. 165, 400-431 (2006).

[13] Lodders, K., Solar System Abundances and Condensation Temperatures of the Elements. Astrophysical Journal. 591 (2): 1220 (2003).

[14] Hansen, C.J.; Kawaler, S.A.; Trimble, V. Stellar Interiors: Physical Principles, Structure, and Evolution (2nd ed.). Springer. 19-20 (2004).

[15] Aller, L.H. The chemical composition of the Sun and the solar system . Proceedings of the Astronomical Society of Australia. 1: 133 (1968).

[16] Giulia Pagliaroli, Francesco Vissani,Features of Kamiokande-II, IMB and Baksan observations and their interpretation in a two-component model for the signal,Astron.Lett.35:1-6 (2009)

[17] Q.R. Ahmad, et al., "Measurement of the rate of interactions produced by 8B solar neutrinos at the Sudbury Neutrino Observatory," Physical Review Letters 87, 071301 (2001).

[18] E. Andres, et al. (AMANDA Collaboration), The AMANDA Neutrino Telescope: Principle of Operation and First Results, Astropart. Phys. 13, 1 - 2(2000)

[19] V. Flaminio, ANTARES Collaboration, Proc Sci. HEP2005 (2006) 25.

[20] A. Achterberg. te al., First Year Performance of The IceCube Neutrino Telescope. (15 May 2006).

[21] Paolo Desiati., IceCube and Deep Core Selected Results and Perspectives. (October 8-11, 2009).

[22] Chang Hyon Ha, Observation of Atmospheric Neutrino-induced Cascades in IceCube with DeepCore (2011).

[23] T.K. Gaisser and J.S. O'Connell, Interactions of atmospheric neutrinos on nuclei at low energy, Phys. Rev. D 34 3 p822 (1986)

[24] Daniele Fargion and Federica Moscato, Chin. J. Astron. Astrophys. Vol.3 (2003), Suppl., 75-86.

[25] P. Vogel and J.F. Beacom, Angular distribution of neutron inverse beta decay, $nubar_e + p \rightarrow (e^+) + n$,The American Physical Society (1999)

[26] $http://www.ips.gov.au/Solar/1/6/$

[27] $http://umbra.nascom.nasa.gov/SEP/$

[28] Chang Hyon Ha, The First year IceCube-DeepCore Results, arXiv:1201.0801v1. (4 Jan 2012).

[29] $http://fermi.gsfc.nasa.gov/$

[30] National Geophysical Data Center, $http://www.ndgc.noaa.gov/ngdc.html$

VITA

Cheng Guo was born in Kaifeng, a famous tourism city and previous capital of Henan Province, China on the 16th day of October, 1987. He graduated from No. 25 Senior High School of same city in 2006. He entered Shijiazhuang Tiedao University in 2006, where he was awarded his degree of Bachelor of Engineering in June of 2010. He was admitted to the Master of Science program at Southern University of Baton Rouge, Louisiana in August of 2010 to pursue his career in Physics.

APPROVAL FOR SCHOLARLY DISSEMINATION

The author grants to the Southern University Library the right to reproduce, by the appropriate methods, upon request, any or all portions of this thesis.

It is understood that "request" consists of an agreement on the part of the requesting party, that said reproduction will not occur without written approval of the author of this thesis.

The author of this thesis reserves the right to publish freely, in the literature, at any time, any or all the portions of this thesis.

Author _____

Date _____